SURFACE CHEMISTRY

2015 © The Authors, some rights reserved; exclusive licensee American Association for the Advancement of Science. Distributed under a Creative Commons Attribution Non-Commercial License 4.0 (CC BY-NC).

10.1126/sciadv.1400133

Identification of different oxygen species in oxide nanostructures with ^{17}O solid-state NMR spectroscopy

Meng Wang,[1] Xin-Ping Wu,[2] Sujuan Zheng,[1] Li Zhao,[1] Lei Li,[1] Li Shen,[1] Yuxian Gao,[3] Nianhua Xue,[1] Xuefeng Guo,[1] Weixin Huang,[3] Zhehong Gan,[4] Frédéric Blanc,[5,6] Zhiwu Yu,[7] Xiaokang Ke,[1] Weiping Ding,[1] Xue-Qing Gong,[2]* Clare P. Grey,[5,8]* Luming Peng[1]*

Nanostructured oxides find multiple uses in a diverse range of applications including catalysis, energy storage, and environmental management, their higher surface areas, and, in some cases, electronic properties resulting in different physical properties from their bulk counterparts. Developing structure-property relations for these materials requires a determination of surface and subsurface structure. Although microscopy plays a critical role owing to the fact that the volumes sampled by such techniques may not be representative of the whole sample, complementary characterization methods are urgently required. We develop a simple nuclear magnetic resonance (NMR) strategy to detect the first few layers of a nanomaterial, demonstrating the approach with technologically relevant ceria nanoparticles. We show that the ^{17}O resonances arising from the first to third surface layer oxygen ions, hydroxyl sites, and oxygen species near vacancies can be distinguished from the oxygen ions in the bulk, with higher-frequency ^{17}O chemical shifts being observed for the lower coordinated surface sites. $H_2{}^{17}O$ can be used to selectively enrich surface sites, allowing only these particular active sites to be monitored in a chemical process. ^{17}O NMR spectra of thermally treated nanosized ceria clearly show how different oxygen species interconvert at elevated temperature. Density functional theory calculations confirm the assignments and reveal a strong dependence of chemical shift on the nature of the surface. These results open up new strategies for characterizing nanostructured oxides and their applications.

INTRODUCTION

As the only nuclear magnetic resonance (NMR) active oxygen stable isotope, ^{17}O NMR spectra have been collected for a large range of metal oxides (*1*–*3*) and reveal that ^{17}O is extremely sensitive to the local environment of the oxygen, resulting in a wide chemical shift range of more than 1000 ppm (*4*). However, only few reports have been published on nanosized oxides (*5*, *6*) despite their use in numerous applications (*7*, *8*). This is largely a result of the high cost of ^{17}O enrichment, generally necessary because of the low natural abundance of ^{17}O (0.037%) and the difficulties associated with efficient isotopic enrichment of the nanomaterials (for example, heat treatment in ^{17}O-enriched O_2 gas, a common method for ^{17}O enrichment, generally leads to particle sintering). However, the low natural abundance of the bulk also brings new possibilities for selective labeling and detection of specific sites.

NMR spectroscopy, which is sensitive to the short-range order of all the resonant nuclei in the sample investigated, should be ideal to study nanomaterials, where the long-range order is usually interrupted by the surface and other defect sites. At the same time, as one of the most extensively studied nano-oxides, ceria nanostructures have been studied for use in a wide range of applications from solid oxide fuel cells (*9*) and catalysis (*10*) [for example, in catalytic convertors (*11*)] to biological applications (*12*). Therefore, we demonstrate our novel ^{17}O NMR approach with this nanomaterial. In addition to the finding that different oxygen species (oxygen ions in different layers and different surfaces) can be distinguished in ^{17}O NMR, we discover that hydroxyl groups can form through water dissociation on ceria nanoparticles, and this process can be exploited to produce an efficient and selective ^{17}O labeling method for the surface of nanosized oxides.

RESULTS

Ceria nanoparticles were prepared hydrothermally (*13*), and their structures were confirmed by x-ray diffraction (XRD; fig. S1A). Broader peaks were observed in the XRD patterns consistent with the small particle sizes (~3 nm), as indicated by the transmission electron microscopy (TEM) images (fig. S1B). Although the ceria nanoparticles exhibit mostly round-shaped or polyhedral morphology, according to previous experimental observations (*14*) as well as theoretical calculations (*15*), the surfaces are dominated by the thermodynamically most stable (111) face (fig. S1B).

^{17}O enrichment was conducted by heating the ~3-nm nanoparticles in an $^{17}O_2$ gas atmosphere at different temperatures. The mean diameters, calculated on the basis of the XRD data by using the Debye-Scherrer equation, increase with increasing enrichment temperature (fig. S2 and table S1) from about 4 to 42 nm after calcination at 523 and 1073 K, respectively. The results are consistent with Brunauer-Emmett-Teller (BET) surface area data (table S2), which show a drop in surface area from 190 to 6 $m^2\ g^{-1}$ over the same temperature range.

The ^{17}O magic angle spinning (MAS) NMR spectra of the ceria nanoparticles are compared with the "bulk" ceria, that is, micrometer-sized

---

[1]Key Laboratory of Mesoscopic Chemistry of Ministry of Education, School of Chemistry and Chemical Engineering, Nanjing University, Nanjing 210093, China. [2]Key Laboratory for Advanced Materials, Centre for Computational Chemistry and Research Institute of Industrial Catalysis, East China University of Science and Technology, 130 Meilong Road, Shanghai 200237, China. [3]Department of Chemical Physics, University of Science and Technology of China, Hefei 230026, China. [4]National High Magnetic Field Laboratory, 1800 East Paul Dirac Drive, Tallahassee, FL 32310–3706, USA. [5]Department of Chemistry, University of Cambridge, Lensfield Road, Cambridge CB2 1EW, UK. [6]Department of Chemistry and Stephenson Institute for Renewable Energy, University of Liverpool, Crown Street, Liverpool L69 7ZD, UK. [7]High Magnetic Field Laboratory, Chinese Academy of Sciences, Hefei 230031, China. [8]Department of Chemistry, Stony Brook University, Stony Brook, NY 11974–3400, USA.
*Corresponding authors. E-mail: luming@nju.edu.cn (L.P.); xgong@ecust.edu.cn (X.-Q.G.); cpg27@cam.ac.uk (C.P.G.)

$Ce^{17}O_2$ particles (commercial reagent CeO_2 obtained from Sinopharm Chemical Reagent Co. Ltd. enriched in $^{17}O_2$ gas; also see figs. S1 and S3), in Fig. 1A. Bulk ceria contains one sharp resonance at 877 ppm corresponding to the four-coordinated oxygen ion (OCe_4) site, consistent with previous studies (*16*). The resonances are much broader for the nanoparticles, and three additional peaks at about 1040, 920, and 825 ppm are observed. The positions of these resonances do not change in spectra acquired with different external magnetic fields (14.1 versus 9.4 T), indicating that these peaks arise from species with small quadrupolar coupling constants (C_Qs). The intensities of the three new peaks decrease (relative to the resonance at 877 ppm) with increasing particle sizes, suggesting that these species are related to surface and subsurface sites or other defect sites (for example, sites near oxygen vacancies) (*17*). The width of these peaks must reflect the large distribution of chemical shifts for the different surface and subsurface environments, as well as the relatively wide size distribution of the nanosized sample (fig. S1). The longitudinal relaxation times (T_1) associated with the new peaks are shorter than that of the bulk environment, again implying that these sites may be nearby defects (fig. S4).

First-principles density functional theory (DFT) calculations were performed to aid the spectral assignments. The $CeO_2(111)$ surface was considered initially (on the basis of the TEM results), and a slab model composed of 6 layers of cerium and 12 layers of oxygen ions (6 CeO_2 trilayers) was constructed for the calculations (Fig. 1B), where the oxygen ions at the same layer have the same local bonding environments and thus have the same chemical shift (δ_{iso}), C_Q, and asymmetry parameter (η_Q) within each layer. The oxygen ions in the center layers (fourth to ninth layers) have similar calculated chemical shifts of ~880 ppm (Fig. 1B), which are close to the experimental chemical shift of oxygen ions in bulk ceria (877 ppm, Fig. 1A) (*16*). For the top and bottom three layers, however, different chemical shifts at about 1033, 921, and 837 ppm (with small C_Q values smaller than 0.14 MHz, table S3) were calculated for oxygen ions at the first, second, and third layers of the slab, respectively. These chemical shift values are surprisingly close to those of the three additional peaks observed in NMR spectra of the ceria nanoparticles. On this basis, the peaks at 1040, 920, and 825 ppm (Fig. 1A) can be tentatively assigned to the oxygen ions at the outmost first, second, and third layers of the particles, respectively. Previously, the dependence of chemical shift on the atomic position with respect to the surface was predicted and observed experimentally only in ^{77}Se NMR of ZnSe nanoparticles; however, the peaks, owing to different layers, were not clearly resolved (*18*). The assignment of the peak at 1040 ppm to the first-layer (three-coordinated) oxygen [on the (111) surface] is in agreement with the trend that the oxygen chemical shift moves to higher frequency as the coordination number decreases in simple metal oxides (*3*). The fractions of first-layer oxygen ions (extracted by using spectral deconvolution) are in accordance with the predictions from BET measurements (fig. S5). The quadrupolar coupling constants of these oxygen ions predicted from DFT calculations are also small (table S3, ν_Q smaller than the radio frequency field amplitude ν_1 of 62.5 kHz).

Calculations were also performed for other low-index surfaces, such as the (110) and (100) surfaces (fig. S6), which may also be present in the nanoparticles. In all the surfaces explored, the oxygen ions on the first layer have lower coordination numbers and give rise to shifts at higher frequencies (>1000 ppm), which is again in agreement with the trend that the oxygen chemical shift appears at a higher frequency with less coordination numbers in simple metal oxides (*3*). The shift calculated for the (110) surface sites is 1061 ppm, somewhat similar to the value for the (111) surface. Different shifts of about 1129 ppm were, however, calculated for the (100) surface sites, with the higher-frequency shift arising from the lower O coordination numbers [two-coordinated sites as compared to three-coordinated sites for the (111) and (110) surfaces]. The lack of a resonance in this chemical shift range in our experimental spectra (Fig. 1A) is in agreement with reports that this is the least energetically favorable low-index surface (*15*). The large difference between the calculated chemical shifts for oxygen ions on the (111) and (100) surfaces (that is, 1129 and 1033 ppm), as well as our experimental observations that match well with calculations of (111) facets, suggests that the ^{17}O NMR shift may be able to probe the coordination numbers of the oxygen atoms and the exposed surface planes of nanocrystals, which can be extremely important for their applications (*19*).

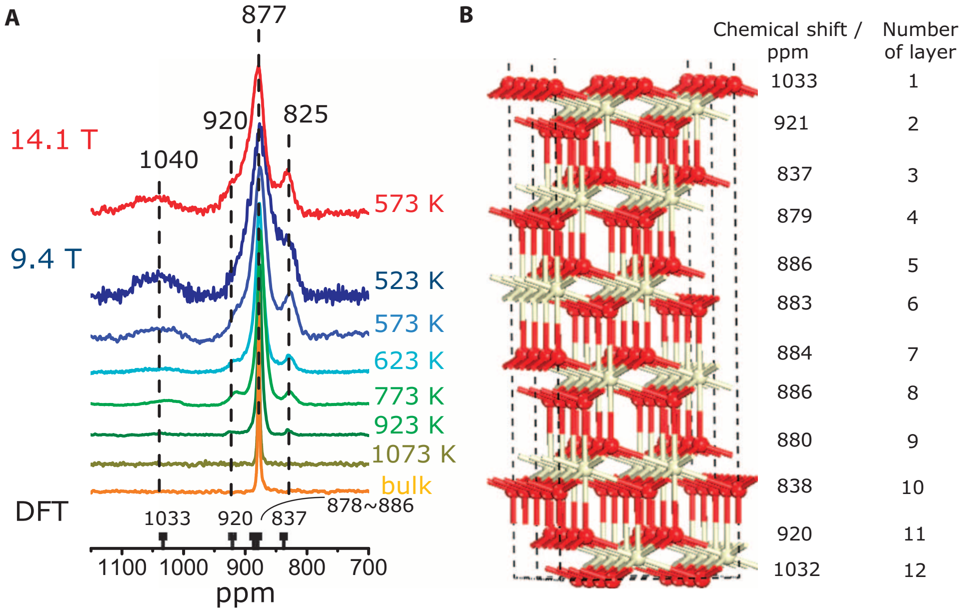

Fig. 1. Solid-state NMR spectra of nanosized ceria in comparison with DFT calculations. (**A**) ^{17}O NMR spectra for ceria nanoparticles enriched at different temperatures and acquired at different external fields compared with the ^{17}O NMR spectra of micrometer-sized ceria (bulk ceria) and the summary of the chemical shifts predicted using a structural model shown in (B). The spectra obtained at 14.1 and 9.4 T were acquired with spinning speeds of 55 and 20 kHz, respectively. Short pulse lengths of 0.1 to 0.4 μs corresponding to π/72 to π/18 pulses for $H_2{}^{17}O$ and optimized recycle delays from 1 to 100 s to ensure quantitative observations of all the resonances were used. Detailed experimental parameters are summarized in table S9. (**B**) The structural model of ceria used in the DFT calculations. Red and white spheres represent oxygen and cerium ions, respectively. The exposed surface is (111), and the calculated chemical shift of ^{17}O in each layer is shown on the right.

To provide additional support for the spectral assignments and to explore the surface structure and chemistry of ceria nanoparticles, natural abundance water was adsorbed on the ^{17}O-enriched ceria samples. The major ^{17}O resonance at 877 ppm from OCe_4 (bulk ceria) remains in the NMR spectra of these samples (Fig. 2A) because the oxygen ions in the bulk are not expected to be affected by surface adsorbates. The resonances at about 1040, 920, and 825 ppm, however, disappear and a new broad shoulder at about 850 ppm can be observed. The shift of this resonance remains unchanged in the spectrum acquired at an ultrahigh field of 19.4 T, indicating that the resonance is associated with a small C_Q (figs. S7 and S8A and table S4). In addition, another broad peak is observed at a much lower frequency (32 ppm). This peak disappears after the sample is dried under vacuum at room temperature, suggesting that this resonance can be assigned to water adsorbed on the surface of ceria. After thermal treatment of the sample at 573 K, the broad peak at 850 ppm disappears and the peaks at 1040, 920, and 825 ppm can be observed again, and the spectrum resembles that of the original bare ceria nanoparticles; this indicates that the structure of the ceria nanoparticles is recovered at elevated temperature when water is completely removed. The resonance at 850 ppm is ascribed to the oxygen ions in the third layer (these environments resonating at 825 ppm in the dry sample), in agreement with DFT calculations (fig. S8 and table S5). The resonances from the oxygen ions on the first and second layers are not observed when water is adsorbed, presumably because of fast exchange between these oxygen ions with water; this hypothesis will be further explored below.

Interactions between ceria nanoparticles and water were also investigated in a reverse way, through the adsorption of ^{17}O-enriched water on nonenriched ceria nanoparticles (preheated at 573 K). On adding $H_2{}^{17}O$ dropwise to ceria nanoparticles at room temperature, weak peaks at about 1040, 877, and 270 ppm appeared (Fig. 2B) in addition to the broad peak at about 32 ppm from adsorbed water. These peaks dominated the spectra after the sample was dried under vacuum at 373 K. Similar spectra were obtained by introducing $H_2{}^{17}O$ to nonenriched ceria nanoparticles calcined at 573 K on a vacuum line (Fig. 2B). The broad resonance at 270 ppm can be tentatively assigned to the hydroxyl groups (Ce^{4+}-^{17}OH) observed previously by Fourier transform infrared (*20*) on the surface of ceria nanoparticles on the basis of the low chemical shift. ^{17}O-^{1}H double-resonance NMR techniques [in this case, cross polarization (CP) (*21*) and rotational echo double resonance (REDOR) (*22*)] were used to confirm this assignment because they can be used to select the ^{17}O resonances of oxygen ions close to protons: they measure the heteronuclear dipolar coupling (that is, between ^{17}O and ^{1}H), a function of distance between ^{17}O and ^{1}H. As seen from Fig. 3A, both the REDOR difference spectrum and CP spectra only show one signal at 270 ppm, confirming that this resonance comes from oxygen ions in close proximity to proton. The NMR parameters of this species, including chemical shift (δ_{iso}) and quadrupolar product [$P_Q = C_Q(1 + \eta_Q{}^2/3)^{1/2}$], were extracted by calculating the frequency change of the center of gravity of the signal at different external fields (300 ppm at 14.1 T versus 270 ppm at 9.4 T). The obtained values (δ_{iso} = 325 ppm, P_Q = 5.1 MHz) are also supported by the DFT calculation results (fig. S8 and table S5). It is clear that the surface hydroxyl groups are associated with much larger C_Q than the less coordinated surface oxygen species, and this is in agreement with the nutation curve (fig. S9). The CP build-up curve (Fig. 3B) shows that with a short contact time (<100 μs), the CP intensity increases rapidly and reaches a maximum at about 90 to 100 μs. With longer contact times, the signal decreases significantly. This CP behavior resembles the oxygen ions at Brønsted acid sites in acidic zeolites (*23*), as well as hydroxyl oxygen species in layered double hydroxides (*24*), indicating that this O species is directly bound to H. ^{1}H-^{17}O TRAPDOR NMR was also used to investigate the ^{1}H-^{17}O dipolar coupling on the surface of ceria nanoparticles (fig. S10). Significant TRAPDOR fraction can be observed at a rather short ^{17}O irradiation time of about 100 μs, and this value reaches maximum at about 140 μs, similar to the observation in acidic zeolite HY (*23*), and again this result suggests that H is directly connected to O. Furthermore, the maximum TRAPDOR effect of ~23% shows the ^{17}O isotopic molar percentage among the surface hydroxyl groups, indicating highly efficient ^{17}O isotopic labeling of the surface of ceria nanoparticles.

The domination of the surface species (that is, the lower coordinated oxygen ions at ~1040 ppm and hydroxyl groups at ~270 ppm) in the spectra of natural abundance ceria nanoparticles adsorbed with ^{17}O water indicates that this approach

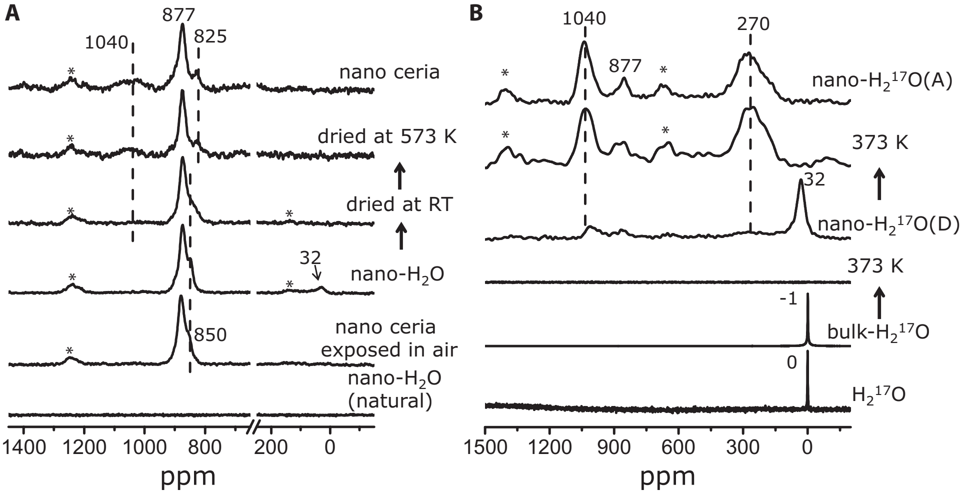

Fig. 2. Solid-state NMR spectra of ceria in contact with water. (**A**, bottom to top) ^{17}O MAS NMR spectra of nonenriched ceria nanoparticles adsorbed with nonenriched water; ceria nanoparticles enriched in $^{17}O_2$ at 573 K and then exposed to air; ceria nanoparticles enriched in $^{17}O_2$ at 573 K and then adsorbed with nonenriched water (water was added dropwise); the previous sample dried under vacuum at room temperature and at 573 K; and ceria nanoparticles enriched in $^{17}O_2$ at 573 K. (**B**, bottom to top) ^{17}O NMR spectra of liquid $H_2{}^{17}O$; ^{17}O MAS NMR spectra of bulk ceria adsorbed with $H_2{}^{17}O$ (bulk-$H_2{}^{17}O$); the previous sample dried under vacuum at 373 K; nonenriched ceria nanoparticles adsorbed with $H_2{}^{17}O$ by adding water dropwise [nano-$H_2{}^{17}O$(D)]; the previous sample dried under vacuum at 373 K; and nonenriched ceria nanoparticles adsorbed with $H_2{}^{17}O$ by adsorbing water through a vacuum line and then dried under vacuum at 373 K [nano-$H_2{}^{17}O$(A)]. The samples of $H_2{}^{17}O$, bulk-$H_2{}^{17}O$, and nano-$H_2{}^{17}O$(D) in (B) were packed into the rotors in air. All the spectra were acquired at 9.4 T. Detailed experimental parameters are summarized in table S10. Asterisks denote spinning sidebands.

can be used as an efficient and surface-selective isotopic enrichment method. To demonstrate this, we use this method to confirm our proposal that the resonances at 1040 and 920 ppm are due to surface and subsurface oxygen sites, specifically those on the (111) surface. To achieve this, we selectively enriched the surfaces of ceria nanorods with $H_2^{17}O$ at room temperature because these are dominated by distinct (111) facets (fig. S11A). Ceria nanorods were also nonselectively enriched in an $^{17}O_2$ atmosphere at 923 K for comparison. Four sharp resonances at 1027, 920, 877, and 825 ppm are seen for the sample enriched in $^{17}O_2$, whereas the peak at 877 ppm due to bulk oxygen species dominates (fig. S11B). For nanorods enriched with $H_2^{17}O$, however, most of the signal comes from two sharp resonances, 1027 and 920 ppm (fig. S11C), confirming our assignment of these resonances to the (111) surface and subsurface sites, respectively. A broad peak with maximum intensity at 270 ppm arising from OH can also be observed in the surface-labeled sample. The broadening seen in the nanoparticles presumably occurs because a larger range of surfaces and disorder is present. This approach shows that selective labeling (*25*), which should be based on water adsorbing/dissociation, can now be controlled to the first few layers of surface sites for oxide nanostructures.

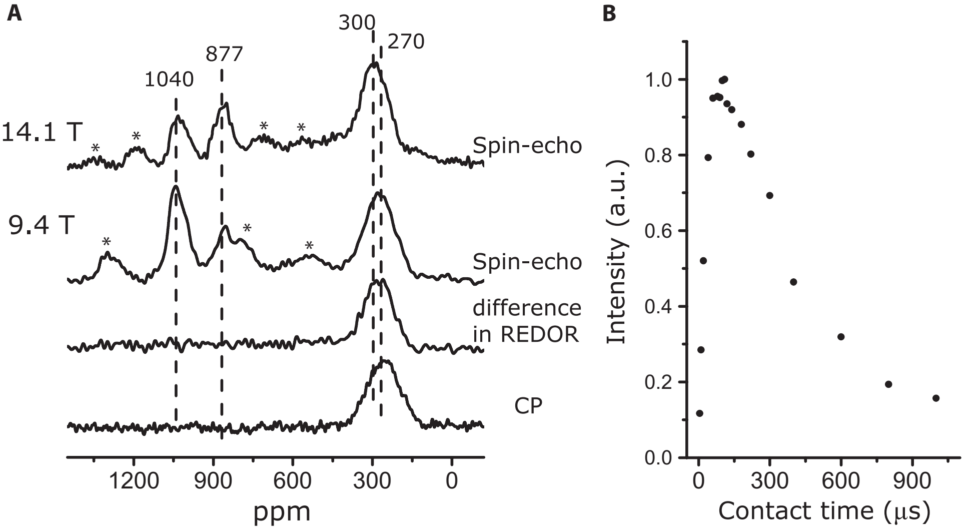

Fig. 3. Double-resonance solid-state NMR data of ceria nanoparticles. (**A**, top to bottom) ^{17}O MAS NMR spectra of ceria nanoparticles adsorbed with ^{17}O water followed by thermal treatment under vacuum at 373 K at 14.1 and 9.4 T; difference spectrum in ^{17}O-^{1}H REDOR experiments; and ^{1}H-^{17}O CP MAS NMR spectrum with a contact time of 100 μs. (**B**) The peak intensity in CP MAS NMR experiment as a function of contact time. Spectra were obtained at both 9.4 and 14.1 T under MAS rates of 13 to 14 kHz. One thousand to 40,000 scans were averaged, and recycle delays from 0.2 to 1 s were used. Asterisks denote spinning sidebands.

The fact that significant surface ^{17}O species were observed only on ceria nanoparticles but not on bulk ceria by adsorbing $H_2^{17}O$ (Fig. 2B) implies that water dissociation readily occurs only at the surface of the more active ceria nanoparticles. Calculations show that the oxygen vacancy formation energies at the outmost first and second layers are substantially smaller than those at the third to sixth layers (fig. S12), suggesting that there are more oxygen vacancies on the first and second layers of ceria. Therefore, water dissociation on ceria nanoparticles is more likely to be the result of water interacting with oxygen vacancies. These observations also agree with the presence of the adsorbed water peak at ~32 ppm when adsorbing nonenriched water on ^{17}O-enriched nanosized ceria. Adsorption of water on nanosized ceria proves effective for ceria nanoparticles with a diameter as large as 16 nm (fig. S13). The relative intensity of the peak at about 270 ppm assigned to the hydroxyl groups decreases with increasing preheating temperature, compared to the peaks at about 1040 and 920 ppm arising from first- and second-layer surface oxygen ions, suggesting that the concentration of oxygen vacancies on the surface of the ceria nanoparticles decreases with increasing particle size.

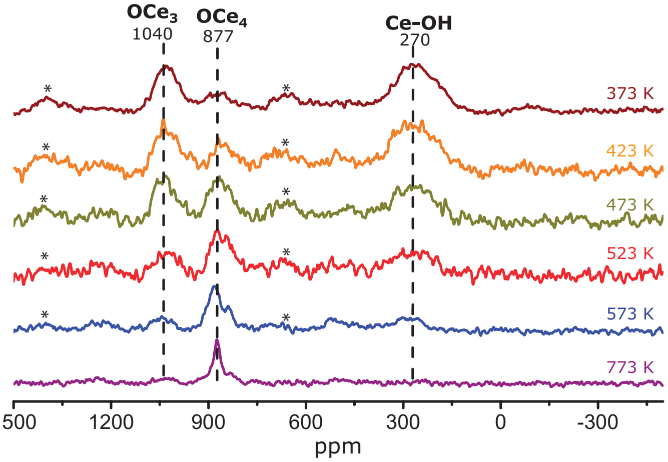

Fig. 4. Solid-state NMR spectra of ceria nanoparticles adsorbed with $H_2^{17}O$ followed by thermal treatment. Top to bottom: ^{17}O NMR spectrum of nonenriched ceria nanoparticles adsorbed with $H_2^{17}O$ by adding water dropwise, then dried under vacuum at 373, 423, 473, 523, 573, and 773 K. A rotor-synchronized Hahn-echo sequence ($\pi/6 - \tau - \pi/3 - \tau$ - acquisition) was used. Spectra were obtained at 9.4 T under a MAS rate of 20 kHz. Eight thousand to 20,000 scans were collected, and recycle delays from 0.2 to 0.5 s were used. Asterisks denote spinning sidebands.

With all the signals being assigned, the evolution of different species on the ceria nanoparticles during thermal treatment was then examined (Fig. 4). At 373 K, the intensities of the peaks from the surface oxygen species (1040 and 270 ppm) are much stronger than that of the peak arising from the oxygen ion in bulk ceria (877 ppm). With increasing temperature, the peaks arising from surface become weaker, whereas the intensity of the peak for bulk oxygen species increases. The latter becomes the major resonance at the temperature above 573 K, indicating that at temperatures higher than 423 K, oxygen ions on the surface can efficiently exchange with oxygen ions in the bulk, presumably through oxygen migration via oxygen vacancies. Nanoparticle sintering can be excluded as a source of the oxygen exchange process, at least at a temperature lower than 573 K, because all of the samples were preheated at 573 K. Therefore, this approach can be used to track the motion of oxygen ions in oxide nanostructures as a function of temperature.

Oxygen vacancies and Ce^{3+} are often present as defects in CeO_2-based materials, and their concentrations are significant in nanoparticles (*17*, *26*), which can be determined by x-ray photoelectron spectroscopy (XPS) (*27*, *28*) (figs. S14 and S15). These species play an important role in controlling the physical properties of this material for a variety of applications, such as heterogeneous catalysis of redox reactions (*29*), and are thus investigated here with NMR. H_2 temperature programmed reduction (TPR) experiments were first carried out on bulk ceria and ceria nanoparticles to determine the temperature to generate Ce^{3+} and oxygen vacancy in H_2 atmosphere (fig. S16). For bulk ceria, a small and relatively narrow H_2 consumption peak can be observed at a temperature lower than 800 K, whereas a much broader and more intense peak centered at 773 K is seen for ceria nanoparticles calcined at 773 K. These peaks can be ascribed to reaction of H_2 with surface oxygen of ceria (*30*). Again, the large peak width associated with the nanoparticles can be ascribed to the wide size distribution of the nanosized sample (fig. S1). The consumption of H_2 increased again at a temperature above 1050 K, which should be associated with the bulk oxygen species. Thus, the ^{17}O NMR spectrum were collected for bulk ceria enriched at 1073 K and then reduced in H_2 atmosphere at 1073 K (Fig. 5A). A shoulder to lower frequency of the OCe_4 peak (877 ppm) and a more distinct lower frequency resonance at about 845 ppm with a full width at half maximum of 12 ppm can be observed. The lower frequency components are tentatively assigned to oxygen ions near the oxygen vacancies or in the Ce^{3+} second cation coordination shell. The spectrum of ceria nanoparticles initially enriched at 773 K and then reduced at 773 K in H_2 also contains a relatively broad resonance with a maximum intensity at about 870 ppm and a broader shoulder at lower frequencies, different from the case of the original nanoparticles (without reduction) or that obtained on reoxidation in oxygen environment (Fig. 5B). The resonance assigned to surface three-coordinated oxygen ions disappears after reduction. Careful examination of these spectra (inset of Fig. 5B) shows that a broader component is present underneath the resonances of the reduced materials. Fermi contact (hyperfine) ^{17}O shifts of more than 728 ppm have been observed for oxygen atoms directly bound to the paramagnetic Ce^{3+} ion, and similarly, large contact shifts are expected in this system (*31*). We ascribe the broad component to oxygen ions in the first coordination cell of one or more Ce^{3+} ions, with the broadening arising from the distribution in local environments and the dipolar interactions between the unpaired electrons centered on Ce^{3+} and ^{17}O.

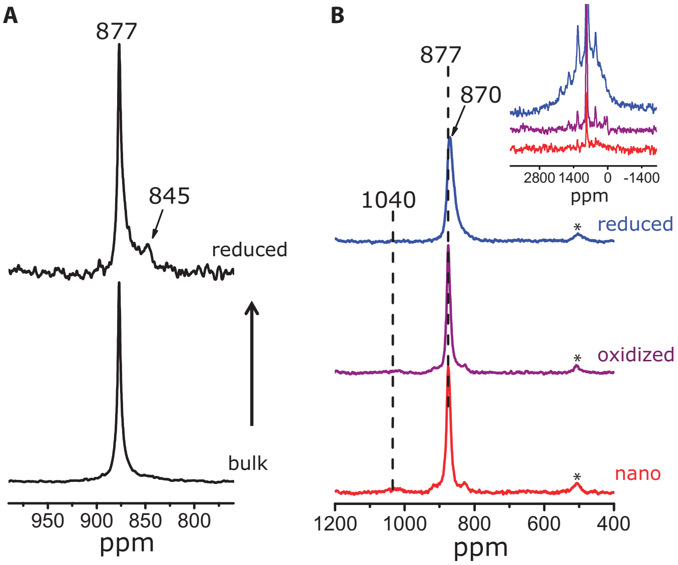

Fig. 5. Solid-state NMR spectra of reduced ceria in comparison with bulk and nanosized ceria. (A) ^{17}O NMR spectra of bulk ceria enriched in $^{17}O_2$ at 1073 K (bottom) and reduced in H_2 atmosphere at 1073 K (top). **(B)** ^{17}O NMR spectra of nanosized ceria enriched in $^{17}O_2$ at 773 K (bottom), reduced in H_2 atmosphere at 773 K (top), and reoxidized in air reduced ceria (middle). Inset shows the full width of the three ^{17}O spectra. A rotor-synchronized Hahn-echo sequence ($\pi/6$ - τ - $\pi/3$- τ - acquisition) was used. Data were obtained at 9.4 T under a MAS rate of 20 kHz. One hundred thousand (A, bulk), 300,000 (A, reduced), 1024 (B), and 40,000 scans (B, inset) were averaged, and recycle delays of 0.1 s (A), 1 s (B), and 0.01 s (B, inset) were used. Asterisks denote spinning sidebands.

We have also calculated the chemical shifts of the environments generated by the presence of the Ce^{3+} ions and oxygen vacancies, and the observation of a sharper peak at a lower frequency is supported by DFT calculations. Three models constructed to describe the reduced ceria were considered: (i) CeO_2 (2 × 2 × 2) unit cell with an oxygen vacancy, which represents the situation of bulk oxygen vacancy; (ii) $CeO_2(111)$ with a subsurface oxygen vacancy; and (iii) $CeO_2(111)$ with a surface oxygen vacancy, with both models (ii) and (iii) representing the situation of vacancies near the surface. All three models contain the two Ce^{3+} ions required to create one oxygen vacancy. The structures of the three models are shown in fig. S17 (A to C), and the calculated chemical shifts are summarized in fig. S17 (D to F) and tables S6 to S8. Generally, the calculated chemical shifts for the oxygen ions 5 Å or closer to the oxygen vacancy in model (i) show a slightly smaller chemical shift compared to the 877 ppm resonance in bulk CeO_2; similar trends are observed for oxygen ions close to a vacancy (that is, in the same layer or the next layer to the oxygen vacancy). The oxygen ions further away show a chemical shift of about 877 ppm. The average chemical shift for the oxygen ions close to an oxygen vacancy is about 845 ppm in the three different structural models. Note that we have not included the additional hyperfine shifts that will result from the presence of the Ce^{3+} ions because these cannot be readily calculated, and so we have only considered the environments that are not in the Ce^{3+} first shell.

DISCUSSION

In conclusion, this paper describes a novel ^{17}O NMR approach to study the surface and defect sites of nanosized oxides. Because the oxygen ions on the surface of ceria nanoparticles (first, second, and third surface layers) show distinct chemical shifts compared to those in the bulk, ^{17}O NMR spectroscopy can be a sensitive probe to monitor the local structure of oxide nanocrystals. Adsorbing water on ceria can be used to explicitly label oxygen ions in the top surface layers (first and second), the method being more controlled than simply heating the nanoparticles at high temperatures. Thus, the method allows for inexpensive ^{17}O enrichment of the surface sites of nanostructures, enabling easy identification of the most active species and monitoring of their behavior in a chemical reaction. Double-resonance NMR techniques can be used to distinguish hydroxyl groups from other surface sites. These methods provide a new strategy to study the unique local structure and surface chemistry of nanostructured oxides, as well as their performance in a wide range of applications. Moreover, we expect that this approach can be used to study the interfaces between oxides and other materials and to illuminate important issues such as the nature of the interactions between the catalytic active species and the support oxides (*32*), as well as the differences in anionic conductivity that are often seen at the interface between two oxides (*33*).

Although the new approach presented allows the detection of the evolution of oxygen species in a chemical process, the exchange of oxygen ions (for example, the process shown in Fig. 4) may limit its applications in monitoring the behavior of oxygen ions in reactions at elevated temperature.

MATERIALS AND METHODS

Study design

The sizes of ceria nanoparticles were determined with the XRD data by using the Debye-Scherrer equation, which were in general agreement with the surface area measurements. There is no rule for stopping NMR data collection in advance, and data acquisition was stopped when enough signal/noise ratio was achieved. Each experimental measurement (sample preparations and NMR experiments) was repeated at least once to ensure that the results can be replicated.

Material preparation

Preparation of ceria nanoparticles. $(NH_4)_2Ce(NO_3)_6$ (1.645 g, 3 mmol, Sinopharm Chemical Reagent Co. Ltd.) was dissolved in distilled water (50 ml), and the mixture was stirred magnetically for 10 min to obtain a good homogeneity. The solution was then transferred into an 80-ml autoclave and heated at 393 K under autogenous pressure for 10 hours before it was allowed to cool to room temperature. The resulting light-yellow precipitates were washed four times with distilled water and anhydrous ethanol and then dried at 353 K for 12 hours.

Preparation of ceria nanorods. The synthesis of CeO_2 nanorods followed the procedure of Mai *et al.* (*34*). In a typical preparation procedure, 1.96 g of $Ce(NO_3)_3{\cdot}6H_2O$ was dissolved in 40 ml of ultrapure water (resistance >18 MW), and 16.88 g of NaOH was dissolved in 30 ml of ultrapure water. The NaOH solution was added dropwise into the $Ce(NO_3)_3$ solution under magnetic stirring at room temperature (RT). The solution was stirred for an additional 30 min at RT and then transferred into a 100-ml Teflon bottle, which was tightly sealed and hydrothermally treated in an autoclave at 373 K for 24 hours and then cooled to RT. The resulting white precipitate was collected, washed with ultrapure water, and dried under vacuum at 353 K for 16 hours. Then, the acquired yellow powder was calcined at 973 K for 4 hours to obtain CeO_2 nanorods.

^{17}O enrichment procedures

Bulk ceria (typically 200 mg, Sinopharm Chemical Reagent Co. Ltd.) and nanosized ceria (typically 200 mg) were first heated at 573 K for 10 hours (except the ceria nanoparticles that were later enriched at 523 K; this particular sample was heated at 523 K) and then enriched by heating the powders in a 70% ^{17}O-enriched O_2 gas (Cambridge Isotope Laboratories) atmosphere at various temperatures (523 to 1073 K) for 10 hours (for bulk ceria sample, ^{17}O enrichment was performed at 1073 K for 10 hours). Ceria nanoparticles were also enriched through introduction of a small amount of 70% ^{17}O-enriched H_2O (Cambridge Isotope Laboratories) by first adding water dropwise or introducing water using a vacuum line at room temperature and then exposing the samples to vacuum to remove additional water. For introducing water using a vacuum line, water vapor (typically 0.1 mmol) was adsorbed onto ceria samples (typically 200 mg) at room temperature for 5 min.

Hydrogen reduction

Ceria samples (typically 200 mg) were reduced under hydrogen (1 bar) in a sealed quartz tube at 773 K for 5 min before allowing them to cool to room temperature under vacuum.

Solid-state NMR spectroscopy

^{17}O MAS NMR spectra were performed on 9.4- and 14.1-T Bruker Avance III spectrometers with 1.3-mm HXY, 3.2-mm HXY, and 4-mm HXY MAS probes (in double resonance) tuned to ^{17}O at 54.2 and 81.3 MHz, respectively. Ultrahigh field data were collected on a 19.6-T Bruker DRX spectrometer with a 1.8-mm single-channel probe tuned to 112.9 MHz. All the samples were packed into the rotors in the N_2 glove box unless otherwise stated. ^{17}O chemical shift is referenced to H_2O at 0.0 ppm.

DFT calculations

The spin-polarized calculations were carried out with the generalized gradient approximation (GGA)–Perdew-Burke-Ernzerhof (PBE) functional, using the Vienna Ab initio Simulation Package (VASP) (*35*), which can calculate chemical shifts for crystalline systems using the linear response method and electric field gradients (EFGs) at the positions of the atomic nuclei. The project-augmented wave method (*36*) was used to describe the electron-core interaction. The Ce (5s, 5p, 6s, 5d, 4f), O (2s, 2p), and H (1s) shells were treated as valence electrons. We used a plane wave kinetic energy cutoff of 500 eV for structure optimization, chemical shift, and EFG calculations. All atoms were allowed to move, and the structural relaxing calculations were converged until the Hellman-Feynman forces on each ion were less than 0.02 eV/Å. For chemical shift and EFG calculations, we used a typically higher stopping criterion of 10^{-8} eV for electronic minimization (fig. S18A). Particularly, to characterize the electronic and geometric structures of ceria properly, we added a Hubbard U of 5 eV in DFT calculations, as suggested by Nolan and co-workers (*37*). Using the PBE + U method, we obtained a lattice parameter of 5.448 Å for bulk ceria, which is in good agreement with the experiment value (5.411 Å) (*38*). The {111}, {110}, and {100} facets of CeO_2 were modeled by surface slabs that are thick enough to maintain trivial fluctuations of chemical shift values in their middle layers, and they were all represented by p(2 × 2) lateral cells (fig. S6, A to C). For $CeO_2(100)$, we removed half of the oxygen atoms from the outermost planes to offset the net dipole and make it stable. To avoid interactions between slabs, they were separated by a vacuum gap greater than 10 Å. The Brillouin zone integration was performed using a 2 × 2 × 1 and 1 × 1 × 1 Monkhorst-Pack grid for surface slabs and the (2 × 2 × 2) bulk cell, respectively. The isotropic chemical shift (δ_{iso}) is defined as $\delta_{iso} = \delta_{ref} + m\delta_{cal}$, where δ_{ref} is the reference chemical shift (fig. S18B), m is a gradient assumed to be equal to −1, and δ_{cal} is the chemical shift value obtained within VASP. The quadrupole coupling constant (C_Q) was calculated as follows:

$$C_Q = \frac{eQV_{zz}}{h},$$

where *e* is the absolute value of the electron charge, *Q* is the element- and isotope-specific quadrupole moment [the experimental value of $Q = -0.02558$ barns (*39*) is used for the ^{17}O], V_{ii} (ii = xx, yy, or zz) is the eigenvalues of the EFG tensor ($|V_{zz}| > |V_{yy}| > |V_{xx}|$), and *h* is the Planck constant.

A chemical shift calculation of clean $CeO_2(111)$ surface was performed without structure relaxing (fig. S18B). The results show that the chemical shifts of oxygen atoms at fifth to eighth O layers have a constant value of 825 ppm. Considering that the bulk oxygen ions have more regular arrangements than the oxygen ions near the surfaces, this constant value can be used to estimate the reference chemical shift value (δ_{ref}). As a result, 52 ppm was taken as the δ_{ref} [$\delta_{ref} = \delta_{iso}(bulk) - m \times \delta_{cal}(bulk) = 877\ ppm - 1 \times 825\ ppm = 52\ ppm$].

SUPPLEMENTARY MATERIALS

Supplementary material for this article is available at http://advances.sciencemag.org/cgi/content/full/1/1/e1400133/DC1

Materials and Methods
Fig. S1. XRD and electron microscopy characterization of ceria nanoparticles.
Fig. S2. XRD patterns of ceria nanoparticles calcined at different temperatures.
Fig. S3. Scanning electron microscopy image of the bulk ceria sample.
Fig. S4. Longitudinal relaxation studies of ceria nanoparticles.
Fig. S5. Quantification of surface oxygen ions from NMR and BET data.
Fig. S6. Chemical shift calculations of ceria with different surface slabs.
Fig. S7. Solid-state NMR of ceria nanoparticles in contact with water at ultrahigh field.
Fig. S8. DFT calculations for ceria in contact with water.
Fig. S9. Nutation NMR of ceria nanoparticles.
Fig. S10. TRAPDOR NMR of ceria nanoparticles.
Fig. S11. Electron microscopy and solid-state NMR spectra of ceria nanorods.
Fig. S12. Vacancy formation energies of different oxygen ions.
Fig. S13. Solid-state NMR spectra of ceria nanoparticles with different surface areas labeled by adsorbing $H_2{}^{17}O$.
Fig. S14. Ce $3d_{3/2,5/2}$ XPS spectra collected for ceria nanoparticles, nanorods, and bulk sample, as well as line fitting results.
Fig. S15. Molar percentage of Ce^{3+} as a function of particle size from XPS data.
Fig. S16. H_2 TPR profiles of bulk ceria and ceria nanoparticles.
Fig. S17. Structure model and chemical shift calculations of ceria with oxygen vacancies.
Fig. S18. The criterion for NMR calculations and the determination of chemical shift.
Table S1. Mean diameter of ceria nanoparticles.
Table S2. BET surface area of ceria samples.
Table S3. Calculated NMR parameters of quadrupolar interaction for ceria.
Table S4. Calculated NMR parameters of quadrupolar interaction for ceria in contact with water.
Table S5. Calculated chemical shifts for ceria in contact with water.
Table S6. Calculated chemical shifts for ceria with oxygen vacancies in the bulk.
Table S7. Calculated chemical shifts for ceria with subsurface oxygen vacancies.
Table S8. Calculated chemical shifts for ceria with surface oxygen vacancies.
Table S9. Detailed NMR parameters for acquiring ^{17}O MAS NMR data in Fig. 1.
Table S10. Detailed NMR parameters for acquiring ^{17}O NMR data in Fig. 2.

REFERENCES AND NOTES

1. T. J. Bastow, S. N. Stuart, ^{17}O NMR in simple oxides. *Chem. Phys.* **143**, 459–467 (1990).
2. S. Yang, K. D. Park, E. Oldfield, Oxygen-17 labeling of oxides and zeolites. *J. Am. Chem. Soc.* **111**, 7278–7279 (1989).
3. K. J. D. MacKenzie, M. E. Smith, Multinuclear Solid-State Nuclear Magnetic Resonance of Inorganic Materials (Elsevier, Oxford, 2002), vol. 6.
4. S. E. Ashbrook, M. E. Smith, Solid state ^{17}O NMR—An introduction to the background principles and applications to inorganic materials. *Chem. Soc. Rev.* **35**, 718–735 (2006).
5. E. Scolan, C. Magnenet, D. Massiot, C. Sanchez, Surface and bulk characterisation of titanium–oxo clusters and nanosized titania particles through ^{17}O solid state NMR. *J. Mater. Chem.* **9**, 2467–2474 (1999).
6. A. V. Chadwick, I. J. F. Poplett, D. T. S. Maitland, M. E. Smith, Oxygen speciation in nanophase MgO from solid-state ^{17}O NMR. *Chem. Mater.* **10**, 864–870 (1998).
7. P. G. Bruce, B. Scrosati, J.-M. Tarascon, Nanomaterials for rechargeable lithium batteries. *Angew. Chem. Int. Ed.* **47**, 2930–2946 (2008).
8. A. T. Bell, The impact of nanoscience on heterogeneous catalysis. *Science* **299**, 1688–1691 (2003).
9. P. Seungdoo, J. M. Vohs, Direct oxidation of hydrocarbons in a solid-oxide fuel cell. *Nature* **404**, 265 (2000).
10. J. A. Rodriguez, S. Ma, P. Liu, J. Hrbek, J. Evans, M. Perez, Activity of CeO_x and TiO_x nanoparticles grown on Au(111) in the water-gas shift reaction. *Science* **318**, 1757–1760 (2007).
11. J. Kašpar, P. Fornasiero, M. Graziani, Use of CeO_2-based oxides in the three-way catalysis. *Catal. Today* **50**, 285–298 (1999).
12. R. W. Tarnuzzer, J. Colon, S. Patil, S. Seal, Vacancy engineered ceria nanostructures for protection from radiation-induced cellular damage. *Nano Lett.* **5**, 2573–2577 (2005).
13. C. Tyrsted, K. M. Jensen, E. D. Bojesen, N. Lock, M. Christensen, S. J. Billinge, B. Brummerstedt Iversen, Understanding the formation and evolution of ceria nanoparticles under hydrothermal conditions. *Angew. Chem. Int. Ed.* **51**, 9030–9033 (2012).
14. K. Zhou, X. Wang, X. Sun, Q. Peng, Y. Li, Enhanced catalytic activity of ceria nanorods from well-defined reactive crystal planes. *J. Catal.* **229**, 206–212 (2005).
15. Y. Jiang, J. B. Adams, M. van Schilfgaarde, Density-functional calculation of CeO_2 surfaces and prediction of effects of oxygen partial pressure and temperature on stabilities. *J. Chem. Phys.* **123**, 064701 (2005).
16. N. Kim, J. F. Stebbins, Vacancy and cation distribution in yttria-doped ceria: An ^{89}Y and ^{17}O MAS NMR study. *Chem. Mater.* **19**, 5742–5747 (2007).
17. S. Tsunekawa, R. Sivamohan, S. Ito, A. Kasuya, T. Fukuda, Structural study on monosize CeO_{2-x} nano-particles. *Nanostruct. Mater.* **11**, 141–147 (1999).
18. S. Cadars, B. J. Smith, J. D. Epping, S. Acharya, N. Belman, Y. Golan, B. F. Chmelka, Atomic positional versus electronic order in semiconducting ZnSe nanoparticles. *Phys. Rev. Lett.* **103**, 136802 (2009).
19. X. Xie, Y. Li, Z. Q. Liu, M. Haruta, W. Shen, Low-temperature oxidation of CO catalysed by Co_3O_4 nanorods. *Nature* **458**, 746–749 (2009).
20. A. Badri, C. Binet, J.-C. Lavalley, An FTIR study of surface ceria hydroxy groups during a redox process with H_2. *J. Chem. Soc. Faraday Trans.* **92**, 4669–4673 (1996).
21. A. Pines, M. G. Gibby, J. S. Waugh, Proton-enhanced NMR of dilute spins in solids. *J. Chem. Phys.* **59**, 569–590 (1973).
22. T. Gullion, J. Schaefer, Rotational-echo double-resonance NMR. *J. Magn. Reson.* **81**, 196–200 (1989).
23. L. M. Peng, Y. Liu, N. J. Kim, J. E. Readman, C. P. Grey, Detection of Brønsted acid sites in zeolite HY with high-field ^{17}O-MAS-NMR techniques. *Nat. Mater.* **4**, 216–219 (2005).
24. L. Zhao, Z. Qi, F. Blanc, G. Yu, M. Wang, N. Xue, X. Ke, X. Guo, W. Ding, C. P. Grey, L. Peng, Investigating local structure in layered double hydroxides with ^{17}O NMR spectroscopy. *Adv. Funct. Mater.* **24**, 1696–1702 (2014).
25. N. Merle, J. Trebosc, A. Baudouin, I. D. Rosal, L. Maron, K. Szeto, M. Genelot, A. Mortreux, M. Taoufik, L. Delevoye, R. M. Gauvin, ^{17}O NMR gives unprecedented insights into the structure of supported catalysts and their interaction with the silica carrier. *J. Am. Chem. Soc.* **134**, 9263–9275 (2012).
26. J. Spanier, R. Robinson, F. Zhang, S.-W. Chan, I. Herman, Size-dependent properties of CeO_{2-y} nanoparticles as studied by Raman scattering. *Phys. Rev. B Condens. Matter* **64**, 245407 (2001).
27. S. Deshpande, S. Patil, S. V. N. T. Kuchibhatla, S. Seal, Size dependency variation in lattice parameter and valency states in nanocrystalline cerium oxide. *Appl. Phys. Lett.* **87**, 133113 (2005).
28. J. Światowska, V. Lair, C. Pereira-Nabais, G. Cote, P. Marcus, A. Chagnes, XPS, XRD and SEM characterization of a thin ceria layer deposited onto graphite electrode for application in lithium-ion batteries. *Appl. Surf. Sci.* **257**, 9110–9119 (2011).
29. T. Kayama, K. Yamazaki, H. Shinjoh, Nanostructured ceria–silver synthesized in a one-pot redox reaction catalyzes carbon oxidation. *J. Am. Chem. Soc.* **132**, 13154–13155 (2010).
30. M. Boaro, M. Vicario, C. de Leitenburg, G. Dolcetti, A. Trovarelli, The use of temperature-programmed and dynamic/transient methods in catalysis: Characterization of ceria-based, model three-way catalysts. *Catal. Today* **77**, 407–417 (2003).
31. K. Djanashvili, C. Platas-Iglesias, J. A. Peters, The structure of the lanthanide aquo ions in solution as studied by ^{17}O NMR spectroscopy and DFT calculations. *Dalton Trans.* 602–607 (2008).
32. J. A. Farmer, C. T. Campbell, Ceria maintains smaller metal catalyst particles by strong metal-support bonding. *Science* **329**, 933–936 (2010).
33. J. Garcia-Barriocanal, A. Rivera-Calzada, M. Varela, Z. Sefrioui, E. Iborra, C. Leon, S. J. Pennycook, J. Santamaria, Colossal ionic conductivity at interfaces of epitaxial ZrO_2:Y_2O_3/$SrTiO_3$ heterostructures. *Science* **321**, 676–680 (2008).
34. H.-X. Mai, L.-D. Sun, Y.-W. Zhang, R. Si, W. Feng, H.-P. Zhang, H.-C. Liu, C.-H. Yan, Shape-selective synthesis and oxygen storage behavior of ceria nanopolyhedra, nanorods, and nanocubes. *J. Phys. Chem. B* **109**, 24380–24385 (2005).
35. G. Kresse, J. Hafner, Ab initio molecular-dynamics simulation of the liquid-metal–amorphous-semiconductor transition in germanium. *Phys. Rev. B Condens. Matter* **49**, 14251–14269 (1994).
36. P. E. Blöchl, Projector augmented-wave method. *Phys. Rev. B Condens. Matter* **50**, 17953–17979 (1994).
37. M. Nolan, S. Grigoleit, D. C. Sayle, S. C. Parker, G. W. Watson, Density functional theory studies of the structure and electronic structure of pure and defective low index surfaces of ceria. *Surf. Sci.* **576**, 217–229 (2005).
38. E. A. Kümmerle, G. Heger, The structures of C–Ce2$O_{3+\delta}$, Ce_7O_{12}, and $Ce_{11}O_{20}$. *J. Solid State Chem.* **147**, 485–500 (1999).
39. D. Sundholm, J. Olsen, Finite element multiconfiguration Hartree-Fock calculations on carbon, oxygen, and neon: The nuclear quadrupole moments of ^{11}C, ^{17}O, and ^{21}Ne. *J. Phys. Chem.* **96**, 627–630 (1992).

Acknowledgments: We thank P. Shi and C. Tian (High Magnetic Field Laboratory, Chinese Academy of Sciences) and X. Wang, X. Han, and X. Bao (Dalian Institute of Chemical Physics, Chinese Academy of Sciences) for the help with high-field NMR experiments. We also thank J. Miao and S. Li (School of Chemistry and Chemical Engineering, Nanjing University) for the help with DFT calculations. **Funding:** This work was supported by the National Basic Research Program of China (2013CB934800 and 2011CB808505), the National Natural Science Foundation of China (NSFC) (20903056, 21222302, 21322307, and 21073083), NSFC—Royal Society Joint Program (21111130201), Program for New Century Excellent Talents in University (NCET-10-0483), the Fundamental Research Funds for the Central Universities (1124020512), and National Science Fund for Talent Training in Basic Science (J1103310). The ECUST group also thanks the Shanghai Rising-Star Program (12QH1400700) and National Super Computing Centre in Jinan for computing time. F.B. thanks the EU Marie Curie actions for an International Incoming fellowship 2011–2013 (grant no. 275212), Clare Hall, University of Cambridge, UK, for a Research fellowship and the University of Liverpool, UK, for funding. C.P.G. thanks the European Research Council for an Advanced Fellowship. This work was also supported by a Project Funded by the Priority Academic Program Development of Jiangsu Higher Education Institutions. **Author contributions:** M.W., S.Z., L.Z., Y.G., and W.H. carried out the synthesis of ceria nanostructures. M.W., L.L., N.X., and X.G. carried out XRD, electron microscopy, surface area measurement, and other characterizations; M.W., S.Z., L.Z., L.S., and L.P. performed ^{17}O isotope enrichment and collected and analyzed the NMR spectra; M.W., Z.Y., Z.G., F.B., and X.K. collected and analyzed the high-field NMR spectra; X.-P.W. and X.-Q.G. conducted the DFT calculations; M.W., X.-P.W., W.H., W.D., X.-Q.G., C.P.G., and L.P. wrote the manuscript, and all authors discussed the experiments and final manuscript. **Competing interests:** The authors declare that they have no competing financial interests.

Submitted 22 November 2014
Accepted 6 January 2015
Published 20 February 2015
10.1126/sciadv.1400133

Citation: M. Wang *et al*., Identification of different oxygen species in oxide nanostructures with ^{17}O solid-state NMR spectroscopy. *Sci. Adv.* **1**, e1400133 (2015).